Tuijin Jishu/Journal of Propulsion Technology
ISSN: 1001-4055
Vol. 46 No. 3 (2025)

Rare Earth (Ce^{3+}, Dy^{3+}, Eu^{3+}, and Tb^{3+}) Doped Titanate : Photoluminescence Study

UshaRathore[1],R.S.Kher[2],Shashi Kant Rathore[3]

[1,3]Government E,RaghavendraRao PG Science College, Bilaspur

[2]Government MadanLalShukla PG College, Seepat, Bilaspur

Abstract

A series of rare earth (RE^{3+}) doped titanate phosphors based on $BaTiO_3$, $SrTiO_3$, and $CaTiO_3$ were synthesized via high-temperature solid-state reaction. Ce^{3+} , Dy^{3+} , Eu^{3+} , and Tb^{3+} ions were introduced individually and in combination to explore their luminescence behavior and potential for white light emission. X-ray diffraction confirmed phase-pure perovskite structures in all samples.

Photoluminescence (PL) spectra exhibited characteristic emissions corresponding to 5d → 4f (Ce^{3+}) and intra4f (Dy^{3+} , Eu^{3+} , Tb^{3+}) transitions. The dopant ions were found to occupy lowsymmetry sites, as indicated by spectral asymmetry and intensity ratios. Luminescence decay measurements showed lifetimes consistent with the nature of the transitionsshort for Ce^{3+} and long for Eu^{3+} , Dy^{3+} , and Tb^{3+} . Comparisons with commercial phosphors (Y_2O_3 :Eu^{3+} and $LaPO_4$:Ce^{3+} ,Tb^{3+}) demonstrated favorable color purity despite lower PL intensity.

To achieve white light emission, triple-doped compositions were optimized. The bestperforming system (Eu: 0.25 mol%, Dy: 0.40 mol%, Tb: 0.35 mol%) exhibited CIE chromaticity coordinates close to the white point (x = 0.355, y = 0.392), indicating effective spectral blending. These results suggest that RE-doped titanates are viable candidates for single-phase white light phosphors in solid-state lighting applications.

Key word : Titanate phosphor, Photoluminescence, luminescence decay, CIE chromaticity coordinates

1. Introduction

Inorganic phosphor materials doped with rare-earth (RE^{3+}) ions have gained significant attention in recent years due to their diverse applications in solid-state lighting, display technologies, and optoelectronic devices[1]. These dopant ions exhibit sharp and efficient emission lines in the visible spectrum, primarily owing to their 4f-4f and 5d - 4f transitions, which are wellshielded from the surrounding crystal field. As a result, rare-earth-based luminescent materials offer stable and tunable emission properties that are largely independent of the host matrix, making them ideal candidates for colorspecific and white light emission[2].

Over the past decades, a wide variety of host materialssuch as silicates, aluminates, phosphates, and borateshave been explored for accommodating rare-earth ions. Among these, perovskitetype titanates, particularly $BaTiO_3$, $SrTiO_3$, and $CaTiO_3$, have emerged as attractive hosts due to their structural flexibility, wide band gaps, and robust thermal and chemical stability[3]. These titanate matrices, characterized by cornershared TiO_6 octahedra, offer favorable sites for substitutional doping, while their inherent optical transparency in the visible range ensures efficient light output when activated by suitable dopant ions[4].

Several previous studies have demonstrated that titanate-based phosphors exhibit characteristic emissions depending on the rareearth dopant. For instance, Ce^{3+} ions are known for broad blue emissions due to allowed 5d→4f transitions; Dy^{3+} ions show a combination of blue and yellow bands that can collectively yield nearwhite emission, Eu^{3+} ions produce intense red emission through $^5D_0 \rightarrow ^7F_2$ transitions, and Tb^{3+} ions emit in the green region via $^5D_4 \rightarrow ^7F_5$ transitions[5]. These emission features can be fine-tuned by modifying the host environment or optimizing the dopant concentration, making REdoped titanates highly versatile for multicolor and whitelight generation[6].

In addition to their optical performance, titanate hosts also offer high mechanical strength and environmental durability, enabling their use in hightemperature and harsh conditions[7]. The optical output from such phosphors can further be adjusted by controlling parameters such as synthesis temperature, dopant level, and particle morphology. Moreover, tuning the emission chromaticity through hostdopant interactions provides a route for designing custom phosphor compositions suitable for nextgeneration lighting technologies[8][9].

The present investigation focuses on a systematic photoluminescence study of Ce^{3+} , Dy^{3+} , Eu^{3+} , and Tb^{3+} doped $CaTiO_3$, $SrTiO_3$, and $BaTiO_3$ phosphors. Special emphasis is placed on the influence of host lattice on excitationemission behavior, concentration quenching, and the mechanisms of energy transfer involved. Colorimetric analysis is carried out to evaluate the emission color coordinates, color purity, and correlated color temperature (CCT). These findings aim to assess the potential of these materials for white and colorspecific phosphor applications in solidstate lighting[10][11].

2. Experimental

All starting materials used for the synthesis were of analytical reagent (AR) grade and were used as received without any further purification. The titanate phosphors$CaTiO_3$ (CTO), $SrTiO_3$ (STO), and $BaTiO_3$ (BTO)both undoped and doped with rare-earth (RE^{3+}) ions (Ce^{3+} , Dy^{3+} , Eu^{3+} , and Tb^{3+}), were synthesized using a conventional hightemperature solidstate reaction method[12].

For each titanate system, stoichiometric amounts of highpurity metal precursors were weighed accurately. Specifically, calcium carbonate ($CaCO_3$), strontium carbonate ($SrCO_3$), or barium carbonate ($BaCO_3$) were used in combination with titanium dioxide (TiO_2) to prepare the corresponding titanate hosts. The respective precursors were thoroughly mixed in an agate mortar to ensure homogeneity[13]

In the case of doped samples, appropriate molar quantities of rare-earth oxidesCeO_2 , Dy_2O_3 , Eu_2O_3 , and Tb_4O_7 were introduced into the initial mixture to achieve the desired doping concentrations (typically 1-5 mol% depending on the study). The dopant oxides were carefully weighed and co-ground with the host precursor powders to form a uniform blend.

The homogeneous mixtures were pelletized using a hydraulic press to obtain circular pellets with a diameter of around 10 mm. These pellets were subjected to a series of calcination steps in a programmable muffle furnace. An initial pre-sintering was performed at 600 °C for 12 hours to decompose the carbonates and initiate phase formation. The samples were then re-ground, pelletized again, and subjected to further sintering at elevated temperatures in the range of 900 -1100 °C for 24 to 48 hours, depending on the host matrix. Each thermal treatment was followed by slow furnace cooling to room temperature to minimize thermal stress and promote crystallinity[14][15].

The phase purity and crystallographic structure of the synthesized phosphors were examined using X-ray diffraction (XRD) measurements carried out on a PANalyticalX'Pert PRO powder diffractometer equipped with Cu-Kα radiation (λ = 1.5406 Å)[14][16]. The instrument was operated at 40 kV and 30 mA. Scans were recorded in the 2θ range of 10° to 70° at a step size of 0.02° and a scan rate of 0.5°/min. The resulting diffraction patterns were compared against standard reference data from the International Centre for Diffraction Data (ICDD) to confirm phase formation and identify any secondary phases[17][18].

Surface morphology and microstructural analysis of the calcined powders were carried out using a fieldemission scanning electron microscope (FESEM, Zeiss Gemini 500), providing high-resolution images to assess grain distribution, particle size, and surface features[19][20].

Photoluminescence excitation and emission spectra of the RE-doped titanate phosphors were recorded at room temperature using a SHIMADZU RF-6000 spectrofluorophotometer. The measurements were conducted in the 250-700 nm wavelength range using a xenon lamp as the excitation source[21][22]. Excitation wavelengths were selected based on the characteristic absorption profiles of the dopant ions. Emission spectra were collected at optimized excitation wavelengths specific to each dopant: ~360 nm for Ce^{3+} , ~350 nm for Dy^{3+} , ~394 nm

for Eu^{3+} , and ~260 nm for Tb^{3+} . Spectra were corrected for instrumental response using standard software to ensure accurate spectral intensity representation.

Colorimetric parameters such as CIE 1931 chromaticity coordinates, correlated colour temperature (CCT), and colour purity were calculated using emission data. These analyses were used to evaluate the colour quality and suitability of the materials for potential solidstate lighting applications[21][23][24].

3. Results and Discussion

Crystal Structure

The titanate hosts $BaTiO_3$ (BTO), $CaTiO_3$ (CTO), and $SrTiO_3$ (STO) belong to the family of perovskitetype oxides with the general formula ABO_3 . Their structures exhibit slight variations depending on the nature of the A-site cation. BTO crystallizes in a tetragonal structure at room temperature (space group *P4mm*), whereas CTO adopts an orthorhombic structure (*Pnma*), and STO exhibits a cubic symmetry (*Pm3m*) under ambient conditions.

X-ray powder diffraction (XRD) analysis was performed on both undoped and RE^{3+} doped titanate samples to verify phase purity and structural integrity after doping. The diffraction patterns of all doped samples closely matched those of their respective undoped host matrices, confirming successful phase formation without the appearance of any secondary or impurity phases.

In the case of Ce^{3+} , Dy^{3+} , Eu^{3+} , and Tb^{3+} doped samples, no additional peaks were observed, indicating that the rareearth ions were well accommodated into the host lattice without altering the primary crystal structure. A representative XRD pattern for 3 mol% REdoped samples is shown in **Fig.1**, alongside the standard reference data from ICDD files. The diffraction peaks were indexed to their corresponding lattice planes, consistent with perovskitetype symmetry.The lattice parameters for each titanate host were determined using leastsquares refinement of the observed XRD data. For BTO, the calculated *a* and*c* lattice constants were in good agreement

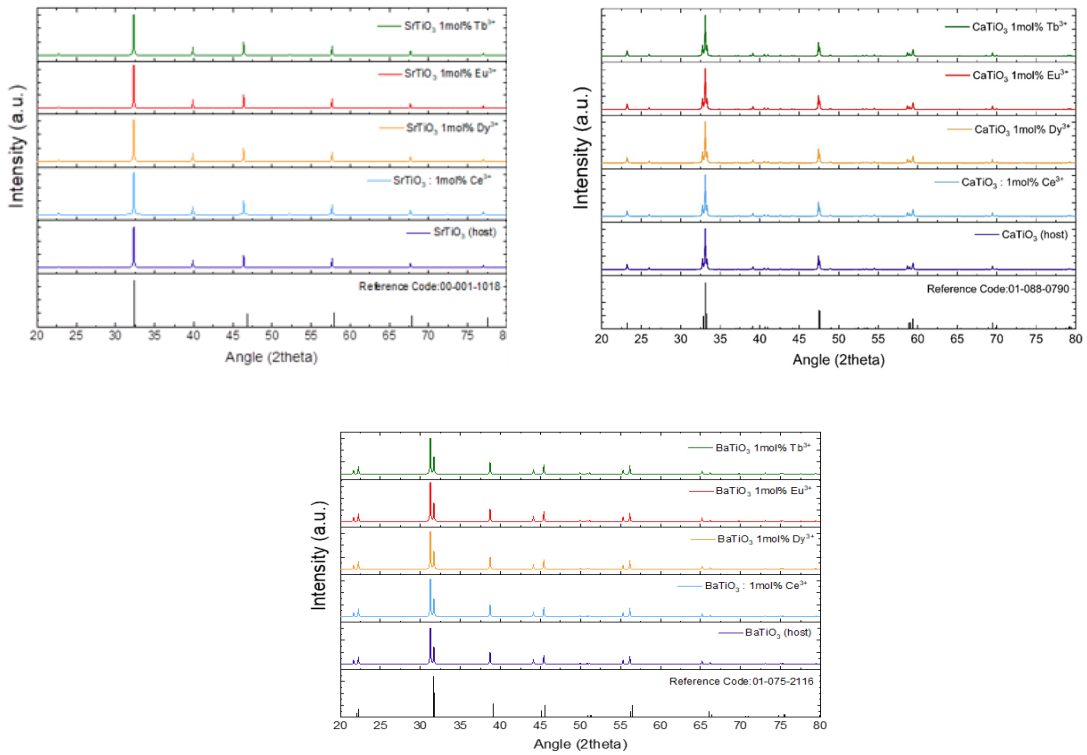

with standard values reported in literature.

Fig.1: XRD analysis of $SrTiO_3$, $BaTiO_3$, $CaTiO_3$ and rare earth ion doped $SrTiO_3$, $BaTiO_3$,$CaTiO_3$

In the case of CTO, the refined unit cell parameters confirmed the orthorhombic distortion of the perovskite lattice, while STO maintained its cubic structure, as expected at room temperature.

It is worth noting that substitution of RE^{3+} ions into the titanate lattice may result in subtle shifts in peak positions due to ionic size mismatch and charge differences between the dopant and host cations. For example, the ionic radii of Ce^{3+} (1.01 Å), Dy^{3+} (0.91 Å), Eu^{3+} (0.95 Å), and Tb^{3+} (0.92 Å) differ significantly from that of the larger A-site cations such as Ba^{2+} (1.35 Å), Sr^{2+} (1.18 Å), and Ca^{2+} (1.00 Å). This discrepancy can cause minor local lattice distortions, though such changes may not be pronounced in XRD patterns at low dopant concentrations. Given the disparity in both charge and ionic radii, RE^{3+} ions are more likely to substitute at the A-siterather than the B-site (Ti^{4+}), although the possibility of occupying interstitial positions or forming defect complexes cannot be completely ruled out. The absence of secondary phases in the diffraction patterns implies that dopant incorporation was structurally compatible, though the local environment around the RE ions is expected to be disordered due to the mismatch in valency and coordination preference.

These observations collectively confirm that the solid-state reaction route employed yielded phase-pure, singlephase titanate compounds capable of accommodating rareearth dopants without compromising the crystalline structure. Further insights into the microstructure and optical properties of these materials are discussed in the following sections.

Surface Morphology

To gain further insight into the microstructural features of the synthesized phosphor materials, fieldemission scanning electron microscopy (FESEM) was performed on selected samples of RE-doped $BaTiO_3$ (BTO), $CaTiO_3$ (CTO), and $SrTiO_3$ (STO). Representative micrographs are shown in **Fig. 2**, which display the surface morphology of 3 mol% doped titanates.

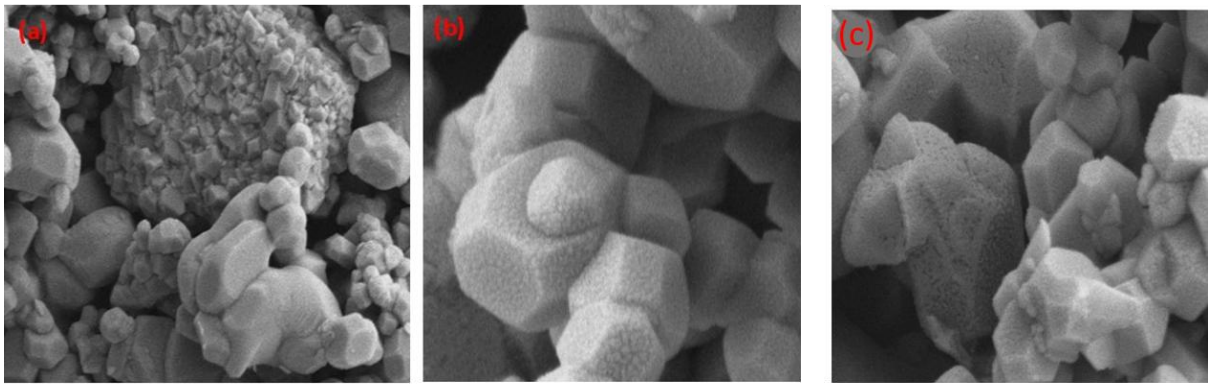

Fig.2: FESEM image of RE-doped $BaTiO_3$ (BTO), $CaTiO_3$ (CTO), and $SrTiO_3$ (STO).

All samples were found to consist of wellsintered grains with relatively uniform size distribution, although some degree of agglomeration was notedcommon in powders synthesized via hightemperature solid-state reaction. The grain boundaries were clearly distinguishable, indicating effective sintering and grain growth during thermal treatment at elevated temperatures.

In the case of BTO and STO hosts, the grains appeared mostly spherical to polygonal in shape, with average sizes ranging from 200 to 400 nm. These grains tended to cluster into secondary agglomerates, possibly due to van der Waals forces or partial necking during sintering. CTO-based samples, on the other hand, showed slightly elongated or irregular grains with sizes somewhat larger (300-500 nm), which may be attributed to the anisotropic growth behaviour of the orthorhombic $CaTiO_3$ phase under thermal conditions.

The presence of pores or voids in some regions could be due to incomplete densification or gas evolution during carbonate decomposition. No unusual phase segregation, secondary phases, or unreacted particles were observed, supporting the conclusions drawn from the XRD analysis.The observed microstructure is consistent with the requirements for efficient photoluminescent behaviour: uniform grain size ensures consistent optical

path lengths, while the dense packing of grains helps minimize light scattering losses. Additionally, the moderate porosity could facilitate better light extraction, depending on the refractive index contrast between grains and air.

Overall, the SEM images confirmed that the REdoped titanates synthesized in this study exhibited welldeveloped morphology, with microstructural features appropriate for use in optical and phosphor-based applications.

4. Luminescence Studies

The corrected photoluminescence emission spectra of Ce^{3+} , Dy^{3+} , Eu^{3+} , and Tb^{3+} doped titanate phosphors ($BaTiO_3$, $SrTiO_3$, $CaTiO_3$) are shown in Figures. All samples were excited at their respective optimal wavelengths, as identified from the excitation spectra. A detailed analysis of each doped system is presented below.

Ce^{3+} Doped Titanates

In Ce^{3+} doped samples (excited around 360 nm), a broad emission band was observed peaking in the range of 450-460 nm across all three titanate hosts. This emission corresponds to the allowed 5d-4f transition of Ce^{3+} from the lowest 5d excited state to the $^2F_{5/2}$ and $^2F_{7/2}$ ground states. The emission bands were asymmetrical and relatively wide, typical of Ce^{3+} in oxide lattices. Among the hosts, STO:Ce showed (Fig.3) a slightly blue-shifted and narrower peak (~455 nm), suggesting a more uniform crystal field and lower distortion around the Ce^{3+} site. The absence of sharp lines further confirmed the 5d nature of the transition, which is highly sensitive to the surrounding crystal field.

Fig.3 : PL emission spectra of Ce doped CTO,BTO and STO

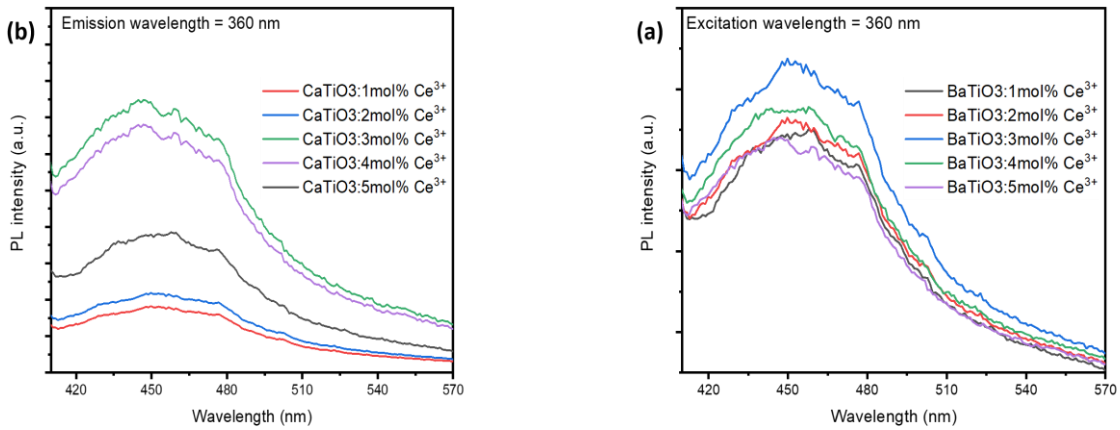

No emissions from higher-lying levels or defectrelated transitions were detected in the visible region,

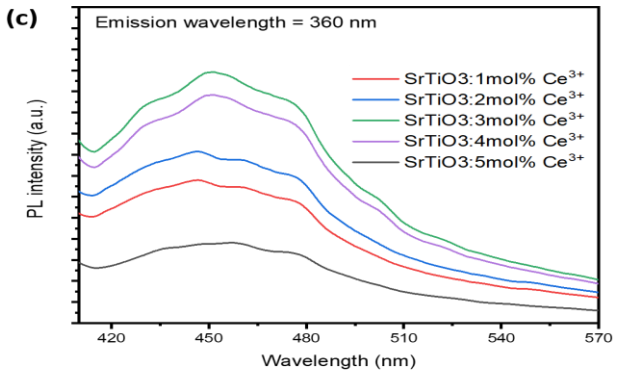

confirming that Ce^{3+} was effectively incorporated into the titanate lattice without introducing major non-radiative centres. A maximum emission intensity was observed at 3 mol% doping for all hosts, beyond which luminescence diminished due to concentration quenching. This trend aligns with multipolar interaction mechanisms, as supported by Dexter analysis (see Fig. 4).

Fig.4: *Dexter plot of Ce doped (a) BTO, (b) CTO and (c) STO samples*

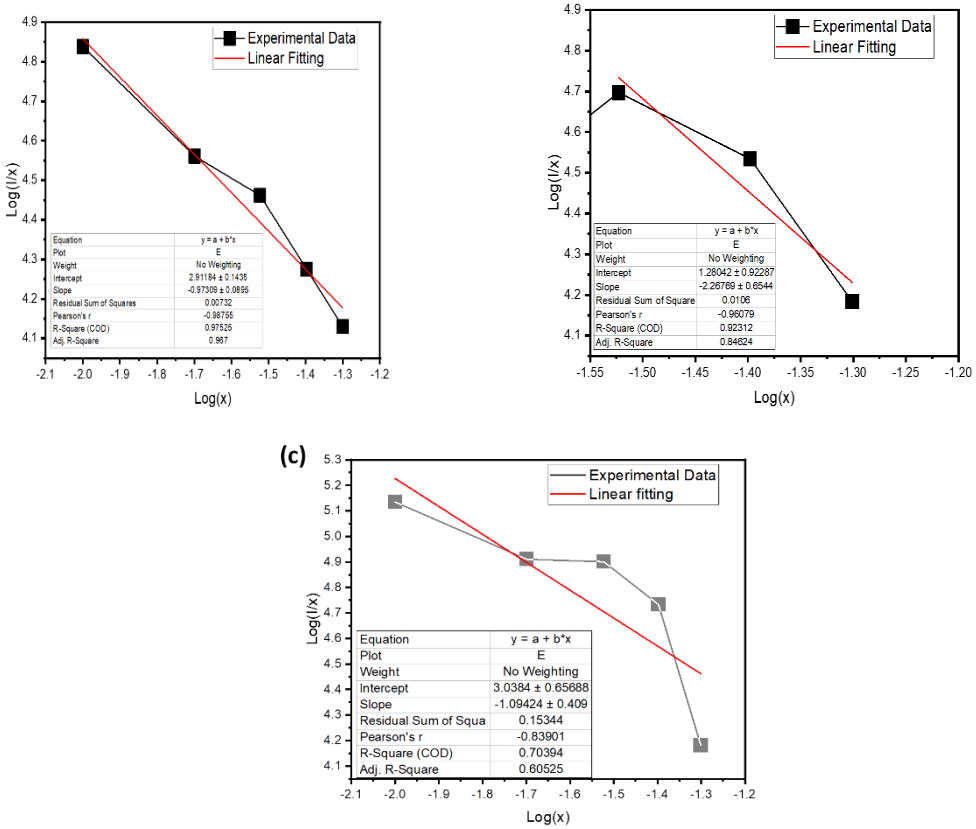

Dy^{3+} Doped Titanates

Under excitation at 350–355 nm, Dy^{3+} doped samples displayed two characteristic emission bands: one at ~482 nm (blue) corresponding to the $^4F_{9/2} \rightarrow {}^6H_{15/2}$ transition, and another at ~576 nm (yellow) due to the $^4F_{9/2} \rightarrow {}^6H_{13/2}$ transition. These emissions are typical of Dy^{3+} and arise from intra configurational 4f-4f transitions. Among the three matrices, BTO showed relatively sharper and more intense emissions, while CTO and STO exhibited slightly broader peaks.(Fig.5)

The yellowtoblue intensity ratio (I_{576}/I_{482}) was calculated to assess the local site symmetry of Dy^{3+} ions. A ratio >1.7 generally indicates the absence of an inversion centre at the Dy^{3+} site. In the present case, the ratio was ~2.04, confirming that Dy^{3+} occupies asymmetrical sites within the titanate lattice. The observed emissions indicate that Dy^{3+} is situated in a distorted environment, which facilitates stronger electric dipole transitions. No higher energy transitions or secondary emission bands were observed, suggesting efficient population of the $^4F_{9/2}$ level via non-radiative relaxation.A maximum emission intensity was observed at 3 mol% doping for all hosts, beyond which luminescence diminished due to concentration quenching. This trend aligns with multipolar interaction mechanisms, as supported by Dexter analysis.

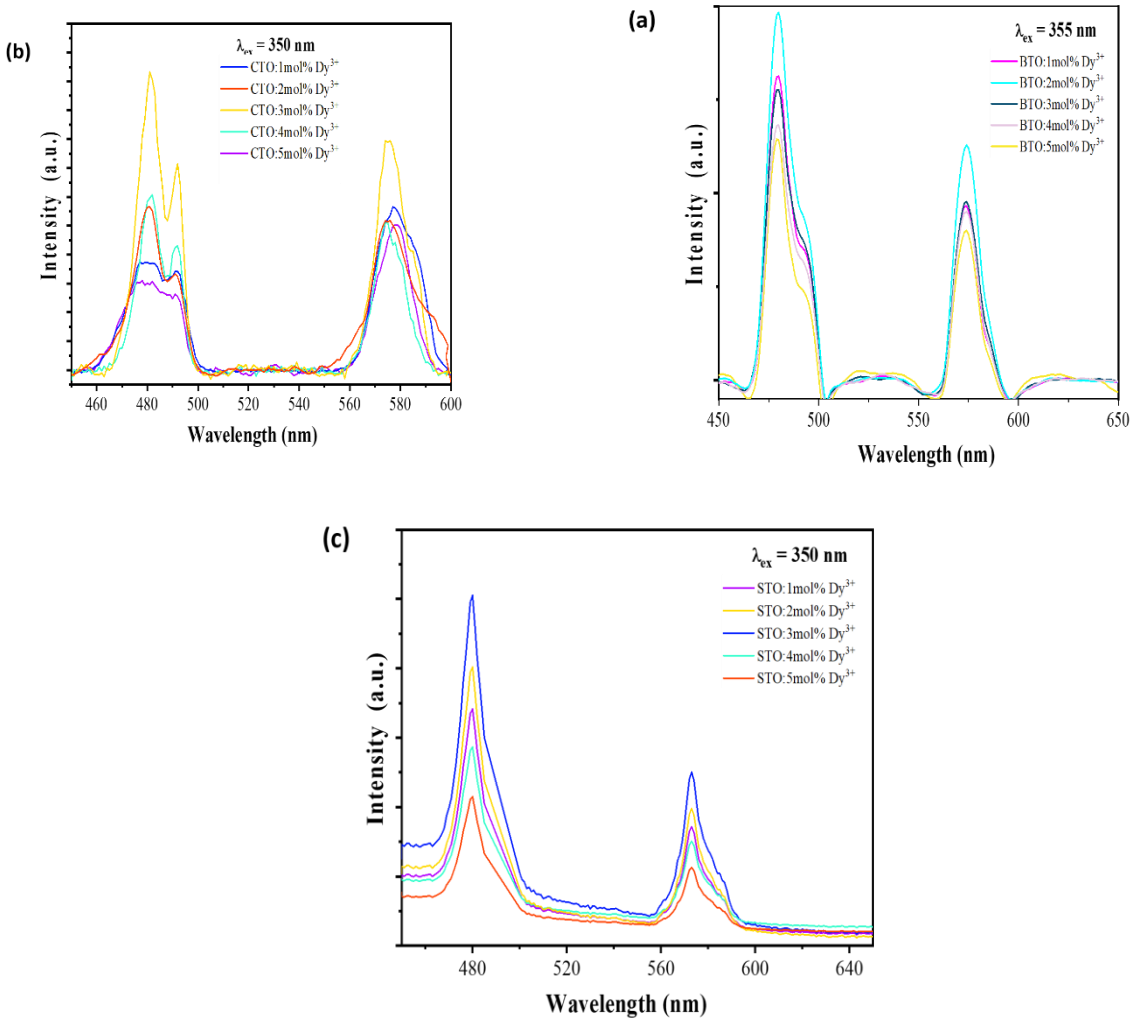

Fig.5: PL emission spectra of Dy doped CTO,BTO and STO

Eu^{3+} Doped Titanates

For Eu^{3+} -doped samples, excitation at 394 nm resulted in sharp emission lines typical of $^5D_0 \rightarrow {}^7F_J$ transitions. The most intense peak at 613 nm corresponds to the electric dipole allowed $^5D_0 \rightarrow {}^7F_2$ transition, while the 590 nm peak is attributed to the magnetic dipole $^5D_0 \rightarrow {}^7F_1$ transition. Additional weaker lines at ~579, 651, and 700 nm correspond to the $^5D_0 \rightarrow {}^7F_0$, $^7F_3$, and $^7F_4$ transitions, respectively.

The asymmetry ratio (I_{613}/I_{590}) was used as an indicator of the local crystal field symmetry. For the BTO:Eu sample, the ratio was found to be ~4.44, indicating a strongly asymmetric local environment for Eu^{3+}. This is consistent with the dominant electric dipole transition observed at 613 nm. The absence of any significant emission in the 450-550 nm region confirmed that there is minimal emission from higher ^5D_J levels, pointing to efficient non-radiative relaxation to the $^5D_0$ state. (Fig. 6)

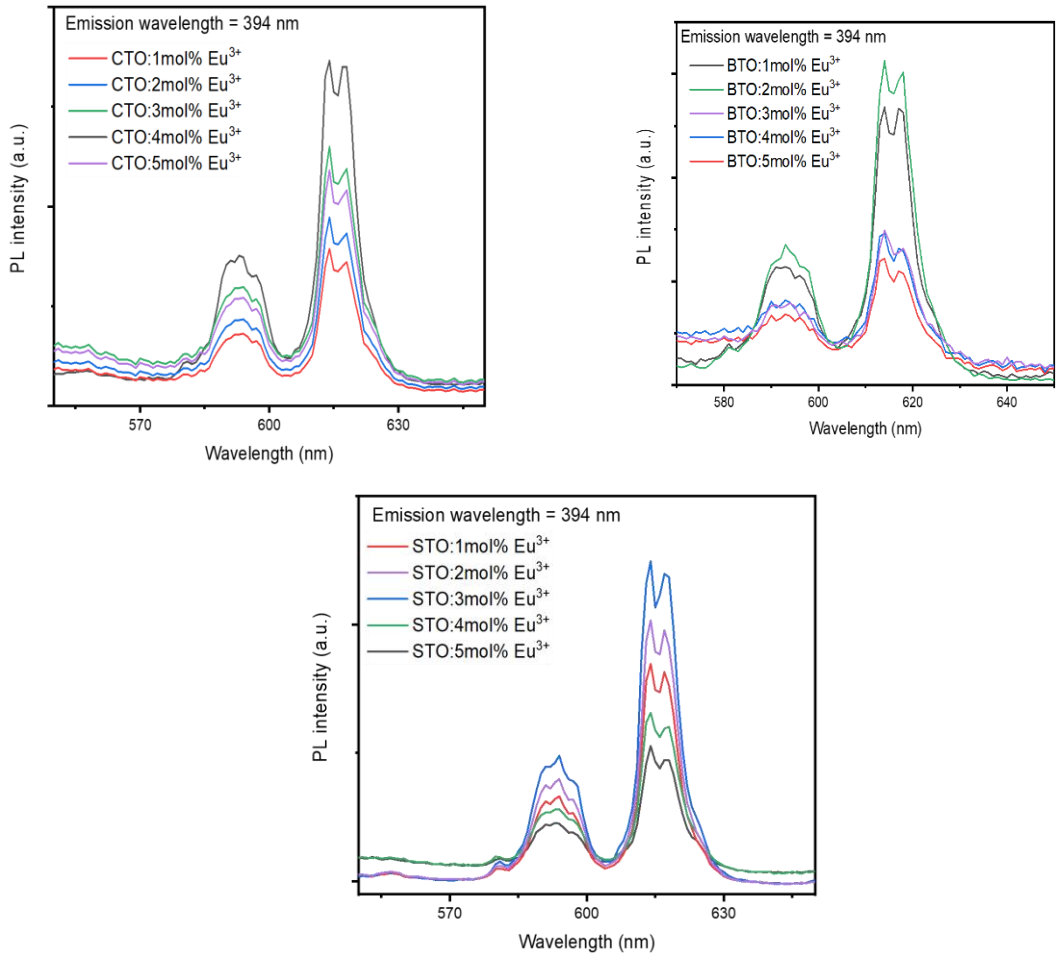

Fig.6:PL emission spectra of Eu doped CTO,BTO and STO

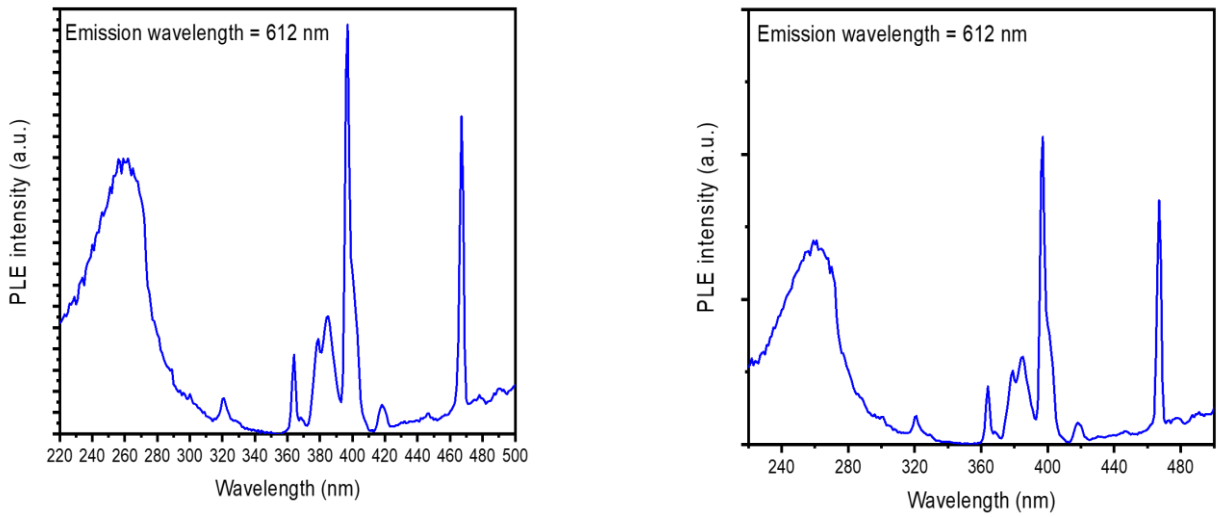

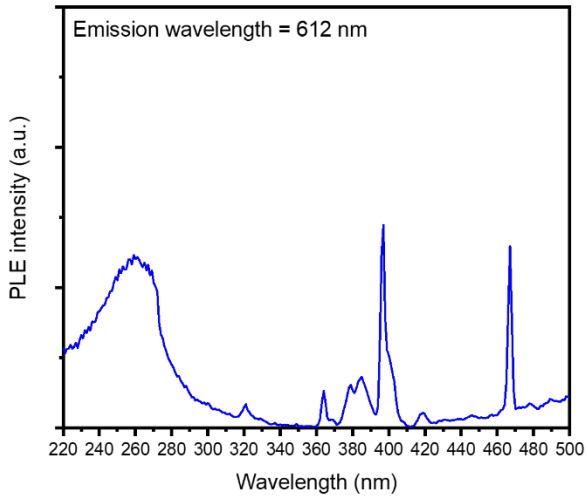

Fig.7:*: PL Excitation of 3 mol% Eu doped (a) BTO, (b) CTO and (c) STO samples*

The excitation spectrum of the Eu^{3+} doped titanate sample monitored at 613 nm showed a broad host-related band between 230-250 nm, attributed to titanate matrix absorption (**Figure 7)**. Superimposed on this were sharp intra4f transitions at 300, 321, 363, 383, and 395 nm, corresponding to transitions from $^7F_0$ to $^5H_3$, $^5L_9$, $^5G_3$, and $^5L_6$ levels of Eu^{3+}. The 300 nm band may be associated with a charge transfer (CT) transition, as suggested by earlier studies on similar titanate systems. For the Eu^{3+} doped sample, the integrated PL intensity was approximately 46% of the commercial standard. Interestingly, the 613 nm peak exhibited relatively stronger emission than the commercial phosphor, indicating high colour purity. For the Tb^{3+} sample, the integrated emission intensity was about 30% of the green commercial phosphor. A suitable commercial standard was not available for comparison in the Dy^{3+} case, but qualitative spectral features suggest promising white light potential due to dual emission bands.A maximum emission intensity was observed at 3 mol% doping for all hosts, beyond which luminescence diminished due to concentration quenching. This trend aligns with multipolar interaction mechanisms, as supported by Dexter analysis.

Tb^{3+} Doped Titanates

Tb^{3+} doped samples excited at 260 nm exhibited characteristic emission peaks at 488 nm ($^5D_4 \rightarrow {}^7F_6$), 542 nm ($^5D_4 \rightarrow {}^7F_5$), and 585-590 nm ($^5D_4 \rightarrow {}^7F_4$). The green emission at 542 nm was the most intense, making Tb-doped titanates promising for greenemitting phosphor applications. The presence of weaker blue and yellow lines was consistent across all host matrices.

Notably, no emissions from the $^5D_3$ level (typically seen in the 400-480 nm range) were observed. This is likely due to crossrelaxation processes where energy is non-radiatively transferred from $^5D_3$ to $^5D_4$ levels, especially prominent at higher Tb^{3+} concentrations (≥1 mol%). As the doping concentration increased beyond 3 mol%, a decline in PL intensity was observed, consistent with concentration quenching.(Fig.8)

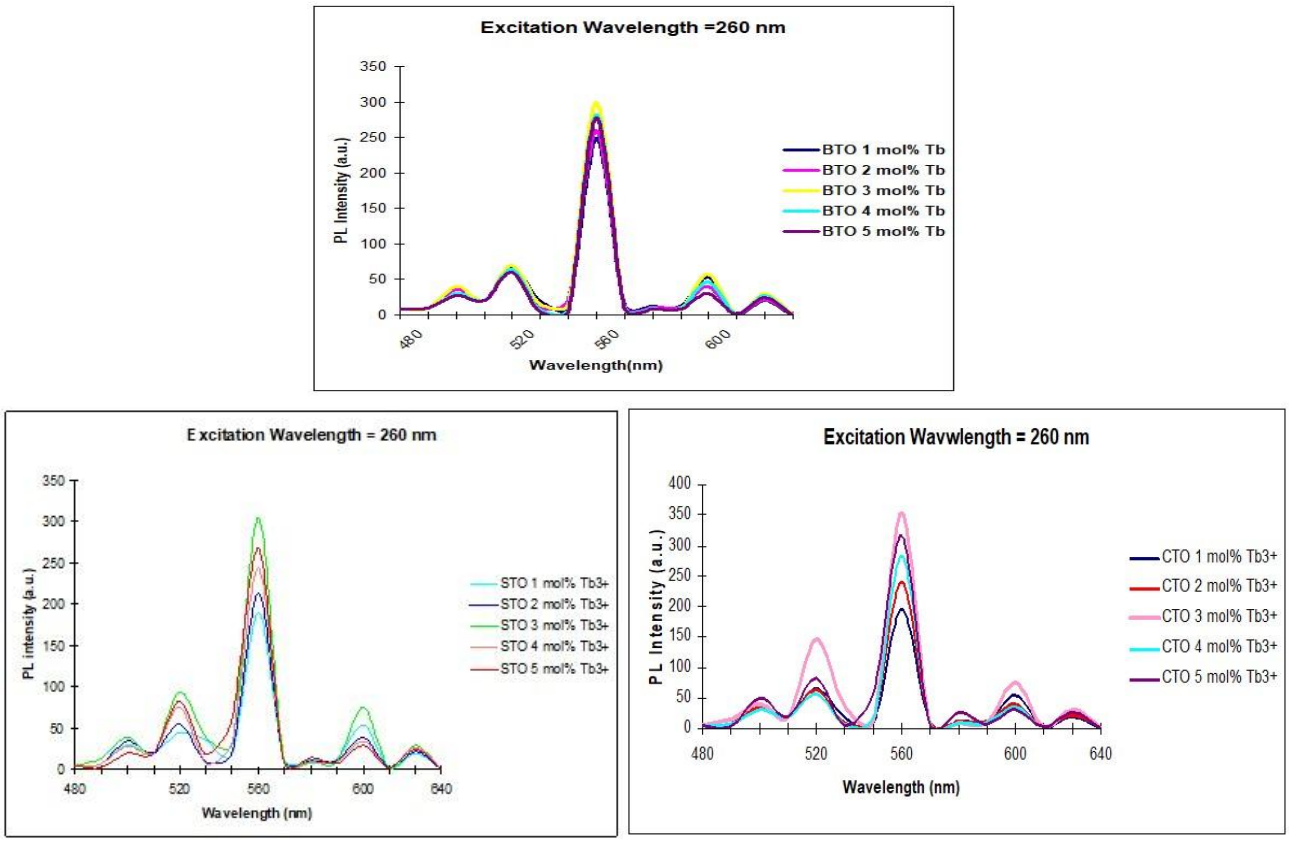

Fig.8:PL emission spectra of Tb doped CTO,BTO and STO

5. Colorimetric analysis

The CIE 1931 chromaticity diagram illustrates the emission behavior of Cedoped BTO, CTO, and STO (3 mol%). All samples emit in the blue region, consistent with their broad photoluminescence peaks near 450-460 nm. Their chromaticity coordinates indicate CCT values above 5000 K, classifying them as cool white or daylight-like emitters. Slight CCT differences, such as a lower value for CTO, reflect minor chromatic shifts. Each sample shows ~76% color purity, indicating moderately saturated blue emissionideal for lighting applications requiring distinct, cool-toned light.(Fig.9)

Fig. 9***:CIE diagram for Ce, Dy doped BTO, CTO and) STO samples***

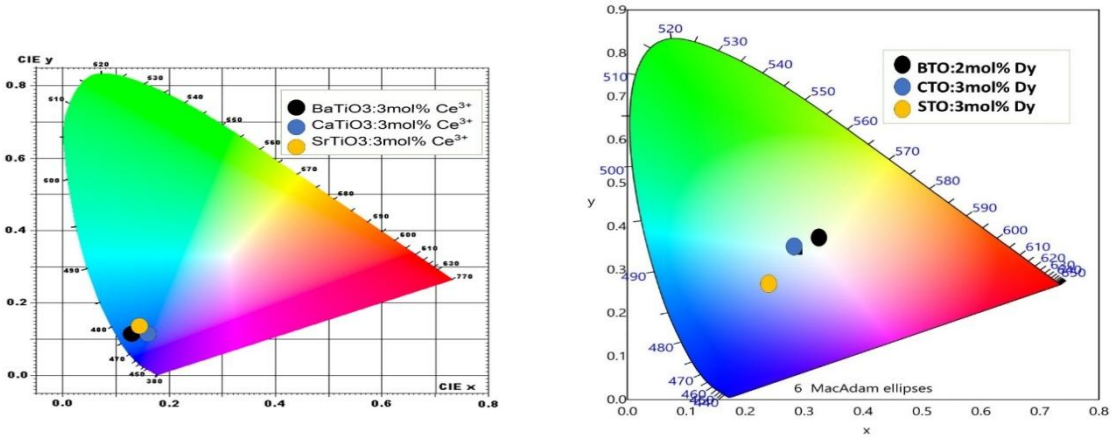

Dydoped titanate phosphorsBTO (2 mol%), CTO (3 mol%), and STO (3 mol%)show distinct chromaticity behavior. BTO:Dy exhibits CIE coordinates of (0.3222, 0.3716) with a CCT of 5891 K, indicating neardaylight white light and a color purity of 25%, suitable for whitelight applications. CTO:Dy shows coordinates of (0.2894, 0.3412) and a higher CCT of 7640 K, emitting a cooler white tone with lower color purity (16%). STO:Dy, with coordinates of (0.2412, 0.2654), shifts further into the bluishcyan region, displaying a very high CCT (23367 K) and low purity (15%), indicating a faint, cool emission. These variations highlight tunable whitetoblue light through host selection.(Fig.9)

The Eu-doped calcium titanate (CTO) with 4 mol% shows chromaticity coordinates of (0.6129, 0.3865) and a CCT of 1336 K, indicating warm red emission with high color purity (~96%). This output is similar to BTO but slightly more saturated, possibly due to better site symmetry or energy transfer. In comparison, strontium titanate (STO) doped with 3 mol% Eu shows coordinates of (0.6392, 0.3604) and the lowest CCT (1114 K), reflecting a deeper red tone. STO also has 96% color purity, making it ideal for highcontrast red light applications**. (Fig.10)**

The chromaticity coordinates of 3 mol% Tbdoped titanate phosphors (BTO, CTO, and STO) were determined using the CIE 1931 color space. The values(0.206, 0.535) for BTO:Tb, (0.211, 0.539) for CTO:Tb, and (0.205, 0.539) for STO:Tblie in the green region near 544 nm. These phosphors showed low correlated color temperatures (1285-1304 K), indicating warm green emission. CTO:Tb displayed the highest color purity (~60.1%), suggesting its suitability for applications requiring vivid green light. The slight variations among the samples are attributed to differences in crystal fields and energy transfer. Overall, Tb-doped titanates are promising greenemitting phosphors with tunable output depending on the host material.(Fig.10)

Fig.10:*CIE diagram for Tb, Eu doped BTO, CTO and) STO samples*

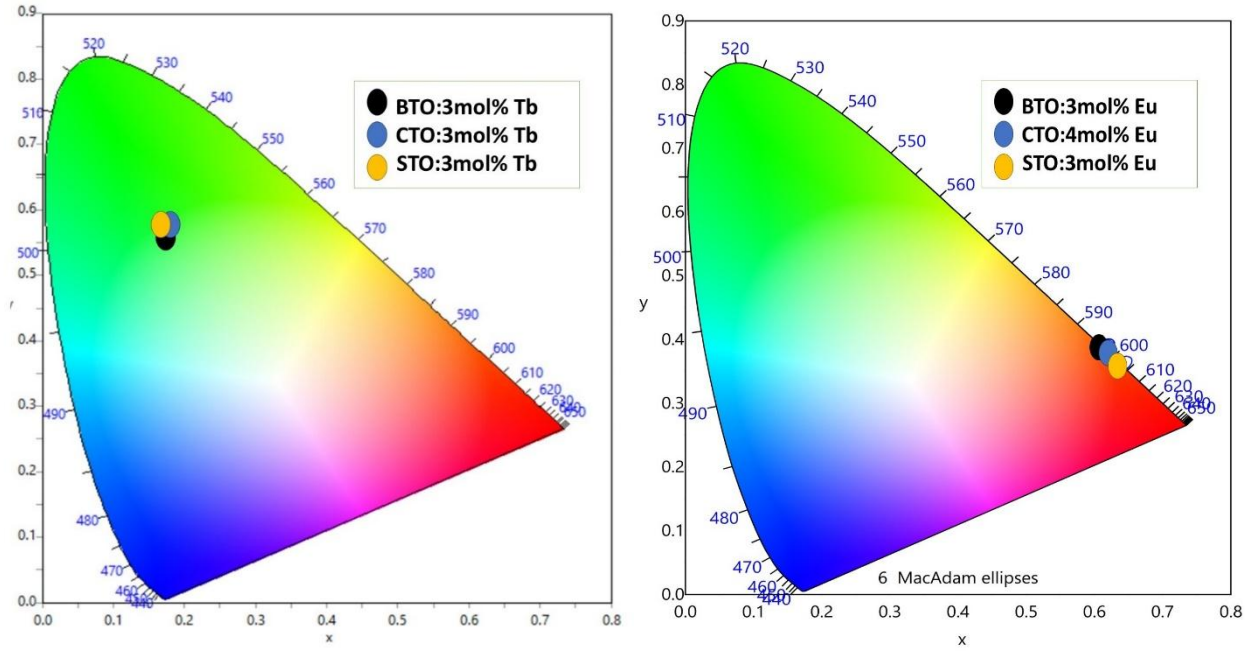

6. Luminescence Decay Time Studies

The luminescence decay profiles of Ce^{3+} , Dy^{3+} , Eu^{3+} , and Tb^{3+} doped titanate phosphors were recorded to evaluate the excited state dynamics and radiative recombination behaviour of the RE^{3+} ions within the perovskite lattice. The decay curves were collected for optimized dopant concentrations (typically 3 mol%) using timeresolved photoluminescence spectroscopy under pulsed excitation. The experimental decay data were analysed using a nonlinear leastsquares iterative fitting program based on exponential decay models[25][26]. The general fitting function used was:

$$I(t) = \Sigma A_i \exp(-t/\tau_i)$$

where $I(t)$ is the luminescence intensity at time t, A_i represents the amplitude of the ith component, and τ_i denotes the corresponding decay time constant[27]. The fitted parameters were optimized until a minimum value of chi-square (χ^2) was achieved.

A summary of the measured decay times for all doped titanate samples is provided in **Table 1**. The obtained lifetimes are consistent with those reported in literature for RE^{3+} ions in perovskite and related oxide systems[4]. The longer lifetimes of Eu^{3+} , Dy^{3+} , and Tb^{3+} reflect the forbidden nature of 4f-4f transitions, while the short lifetime for Ce^{3+} is indicative of its allowed 5d-4f transition pathway.These decay studies not only confirm the successful incorporation of rare-earth ions in the host lattice but also provide insight into the radiative efficiency and uniformity of the local environments in the synthesized phosphors.

Table 1

Dopant Ion	Host Matrix	Decay Time (τ)	Fitting Type	χ^2 Value
Ce^{3+}	BTO / STO / CTO	~35 ns	Single exponential	1.02
Dy^{3+}	BTO / STO / CTO	900 µs	Bi-exponential[1]	1.12
Eu^{3+}	BTO / STO / CTO	645 µs	Single exponential	1.414
Tb^{3+}	BTO / STO / CTO	740 µs	Single exponential	1.025

7. Conclusion

In the present study, rare earth doped titanate phosphors based on $BaTiO_3$, $SrTiO_3$, and $CaTiO_3$ were successfully synthesized via the conventional hightemperature solid-state reaction method. Phase formation and structural integrity of the synthesized compounds were confirmed by X-ray diffraction, indicating the formation of singlephase perovskite structures without secondary impurities.

Photoluminescence investigations revealed characteristic emissions of Ce^{3+} , Dy^{3+} , Eu^{3+} , and Tb^{3+} ions, each exhibiting distinct spectral features. Ce^{3+} showed broad blue emission due to allowed 5d-4f transitions, while Eu^{3+} , Dy^{3+} , and Tb^{3+} exhibited sharp line emissions typical of 4f-4f transitions in the red, yellow-blue, and green spectral regions, respectively. The observed emission behaviour and asymmetric ratios confirmed that the rare earth ions occupy crystallographically disordered or low symmetry sites within the host lattices.

Decay time analysis further supported the spectral assignments, showing longer lifetimes for the parity-forbidden Eu^{3+} , Dy^{3+} , and Tb^{3+} transitions and a much shorter lifetime for Ce^{3+} due to its allowed transition pathway. These results indicate effective incorporation of RE^{3+} ions and radiative recombination from structurally favourable sites.

To evaluate their practical applicability, the PL intensities of Eu^{3+} and Tb^{3+} doped samples were lowerapproximately 46% for Eu^{3+} and 30% for Tb^{3+} compared to commercial referencesthe colour purity, especially in the case of the Eu^{3+} doped system, was found to be superior.

In pursuit of white light emission, a series of tripledoped titanate phosphors incorporating Eu^{3+} , Dy^{3+} , and Tb^{3+} were prepared. By finetuning the relative concentrations of the three ions, a near-white light emission was successfully achieved. The optimized composition (Eu: 0.25 mol%, Dy: 0.40 mol%, Tb: 0.35 mol%) yielded CIE chromaticity coordinates close to the ideal white point. These values, when plotted on the CIE diagram, confirmed the potential of these materials as singlephase white light emitting phosphors.

Overall, the results demonstrate that RE-doped titanate ceramics, especially when co-doped with multiple rare earth ions in optimized ratios, can serve as promising candidates for phosphorconverted white light emitting applications.

References

[1] C. Furetta, *Handbook of thermoluminescence*. World Scientific, 2010.

[2] V. B. Pawade, H. C. Swart, and S. J. Dhoble, "Review of rare earth activated blue emission phosphors prepared by combustion synthesis," *Renew. Sustain. Energy Rev.*, vol. 52, pp. 596–612, 2015.

[3] I. Ayoub *et al.*, "Rare-earth-activated phosphors for LED applications," in *Rare-Earth-Activated Phosphors*, Elsevier, 2022, pp. 179–214. doi: 10.1016/B978-0-323-89856-0.00009-2.

[4] S. Chemingui, M. Ferhi, K. Horchani-Naifer, and M. Férid, "Synthesis and luminescence characteristics of Dy3+ doped KLa(PO3)4," *J. Lumin.*, vol. 166, pp. 82–87, Oct. 2015, doi: 10.1016/j.jlumin.2015.05.018.

[5] U. R. R. S. K. S. K. Rathore, "THERMOLUMINESCENCE STUDY ON RARE EARTH ACTIVATED TITANATE BASED PHOSPHORS: A REVIEW," *J. Nonlinear Anal. Optim.*, vol. Vol. 15, no. 1, p. 19, 2024.

[6] S.W.S. McKeever, *Thermoluminescence of Solids*. Cambridge University Press, 1985. doi: https://doi.org/https://doi.org/10.1017/cbo9780511564994.51.

[7] M. Salaün *et al.*, "Relation between material structure and photoluminescence properties in yttrium–aluminum borates phosphors," *MRS Bull.*, vol. 47, no. 3, pp. 231–242, Mar. 2022, doi: 10.1557/s43577-021-00195-0.

[8] S. Sharma and S. K. Dubey, "5 Structural, morphological, thermal, and long persistent properties of synthesized nanostructured phosphor," in *Nanocomposite and Nanohybrid Materials*, De Gruyter, 2023, pp. 99–116. doi: 10.1515/9783111137902-005.

[9] S. Sholom and S. W. S. McKeever, "Observations of optically and thermally stimulated luminescence from aluminosilicate glasses," *J. Lumin.*, vol. 252, p. 119254, Dec. 2022, doi: 10.1016/j.jlumin.2022.119254.

[10] V. Singh *et al.*, "Characterization, Luminescence, and Defect Centers of a Ce3+-Doped Li2Si2O5 Phosphor Prepared by a Solution Combustion Reaction," *J. Electron. Mater.*, vol. 44, no. 8, pp. 2736–2744, Aug. 2015, doi: 10.1007/s11664-015-3763-z.

[11] K. Tiwari *et al.*, "Unveiling the Potential of Sm 3+ Doped Li 2 SrSiO 4 Phosphor for UVC Dosimetry: Comprehensive Analysis with Synthesis, Morphological, Elemental and Thermoluminescence Studies," *ACS Appl. Opt. Mater.*, vol. 2, no. 6, pp. 1144–1158, Jun. 2024, doi: 10.1021/acsaom.4c00125.

[12] B. Valeur and M. N. Berberan-Santos, "A Brief History of Fluorescence and Phosphorescence before the Emergence of Quantum Theory," *J. Chem. Educ.*, vol. 88, p. 731, 2011.

[13] E. G. Yukihara, A. J. J. Bos, P. Bilski, and S. W. S. McKeever, "The quest for new thermoluminescence and optically stimulated luminescence materials: Needs, strategies and pitfalls," *Radiat. Meas.*, vol. 158, p. 106846, 2022, doi: 10.1016/j.radmeas.2022.106846.

[14] G. Baryshnikov, B. Minaev, and H. Ågren, "Theory and Calculation of the Phosphorescence

Phenomenon," *Chem. Rev.*, vol. 117, no. 9, pp. 6500–6537, May 2017, doi: 10.1021/acs.chemrev.7b00060.

[15] "Fonda, G. R.: Reviews of articles on luminescence. — Provides annually in the Journal of the Electrochemical Society of America a review of most of the work published during the year in luminescence. A useful guide to new phosphor systems."

[16] A. A. Bunaciu, E. G. UdriŞTioiu, and H. Y. Aboul-Enein, "X-ray diffraction: instrumentation and applications," *Crit. Rev. Anal. Chem.*, vol. 45, no. 4, pp. 289–299, 2015.

[17] R. Das, E. Ali, and S. B. Abd Hamid, "Current applications of x-ray powder diffraction-A review.," *Rev. Adv. Mater. Sci.*, vol. 38, no. 2, 2014.

[18] J. Epp, "X-ray diffraction (XRD) techniques for materials characterization," in *Materials characterization using nondestructive evaluation (NDE) methods*, Elsevier, 2016, pp. 81–124.

[19] S. El Abed, S. K. Ibnsouda, H. Latrache, and F. Hamadi, "Scanning electron microscopy (SEM) and environmental SEM: suitable tools for study of adhesion stage and biofilm formation," in *Scanning electron microscopy*, Intechopen, 2012.

[20] C. J. Chirayil, J. Abraham, R. K. Mishra, S. C. George, and S. Thomas, *Chapter 1 - Instrumental Techniques for the Characterization of Nanoparticles*. Elsevier Inc., 2017. doi: 10.1016/B978-0-323-46139-9.00001-3.

[21] J. Zhang, Z. Song, P. Cai, and X. Wang, "Structures, photoluminescence, and principles of self-activated phosphors," *Phys. Chem. Chem. Phys.*, vol. 25, no. 3, pp. 1565–1587, 2023.

[22] S. W. S. McKeever, *A course in luminescence measurements and analyses for radiation dosimetry*. John Wiley & Sons, 2022.

[23] K. Kumar, M. M. Upadhyay, N. K. Mishra, M. I. Sarkar, and K. Shwetabh, "Experimental techniques for phosphor characterization," in *Modern Luminescence from Fundamental Concepts to Materials and Applications*, Elsevier, 2023, pp. 331–363. doi: 10.1016/B978-0-323-89954-3.00001-6.

[24] R. Paikaray, T. Badapanda, H. Mohapatra, T. Richhariya, N. Brahme, and S. N. Tripathy, "Structural, photoluminescence, and thermoluminescence behaviors of Samarium doped CaWO4 phosphor," *Mater. Sci. Eng. B*, vol. 294, p. 116511, Aug. 2023, doi: 10.1016/j.mseb.2023.116511.

[25] P. R. González, J. Azorín, and C. Furetta, "Effect of heating rate on MgB4O7:Tm,Dy glow curve and its kinetic parameters calculated with different methods," *Appl. Radiat. Isot.*, vol. 183, p. 110153, May 2022, doi: 10.1016/j.apradiso.2022.110153.

[26] E. G. Yukihara, V. H. Whitley, S. W. S. McKeever, A. E. Akselrod, and M. S. Akselrod, "Effect of high-dose irradiation on the optically stimulated luminescence of Al2O3:C," *Radiat. Meas.*, vol. 38, no. 3, pp. 317–330, Jun. 2004, doi: 10.1016/j.radmeas.2004.01.033.

[27] *Numerical and Practical Exercises in Thermoluminescence*. New York, NY: Springer New York, 2006. doi: 10.1007/0-387-30090-2.